Structure, Volume *20*

Supplemental Information

Specific, Sensitive, High-Resolution Detection of Protein Molecules in Eukaryotic Cells Using Metal-Tagging Transmission Electron Microscopy

Cristina Risco, Eva Sanmartín-Conesa, Wen-Pin Tzeng, Teryl K. Frey, Volker Seybold, and Raoul J. de Groot

Inventory of Supplemental Information

Figure S1 (related to Figures 1, 2, and 3)

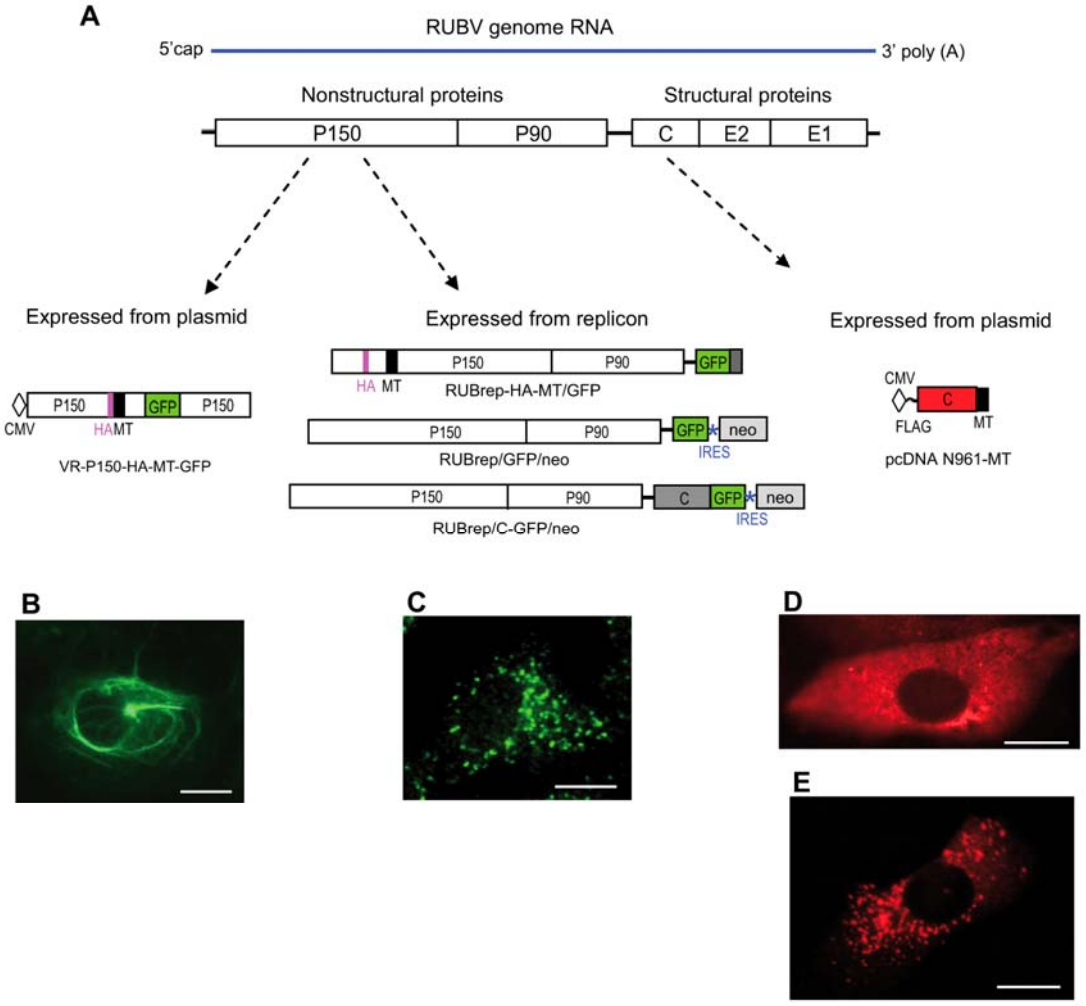

Figure S2 (related to Figures 2, 3, and 4)

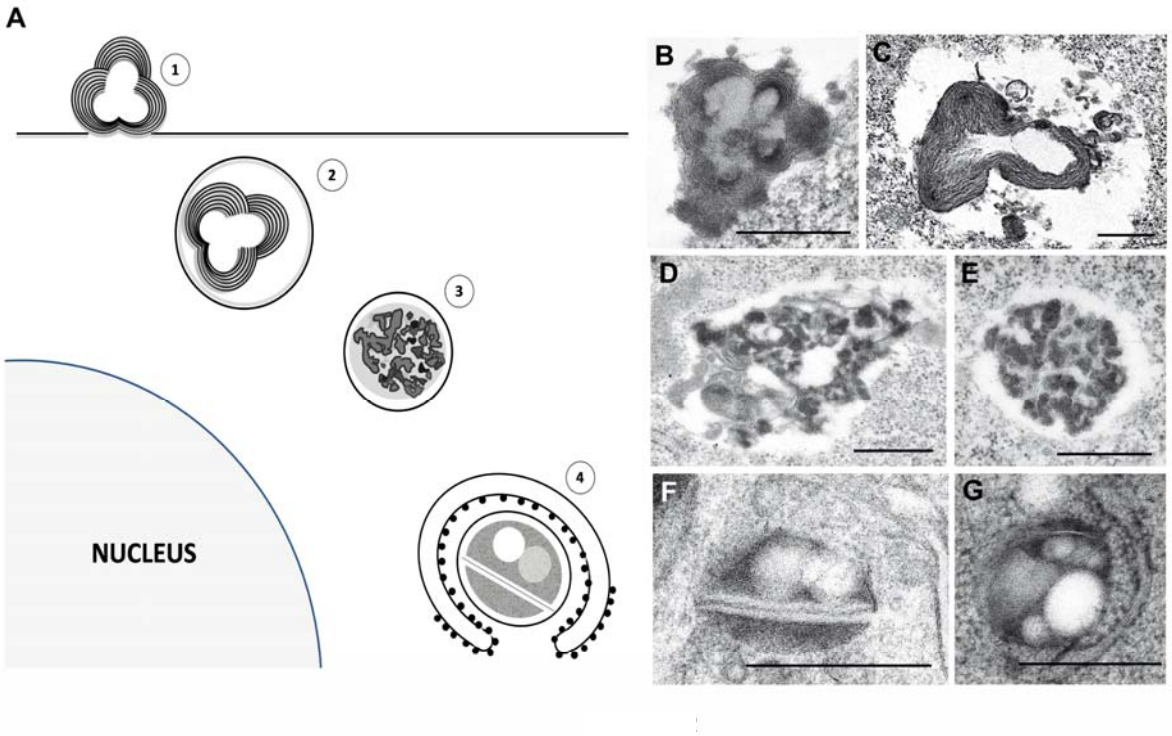

Figure S3 (related to Figures 2 and 3)

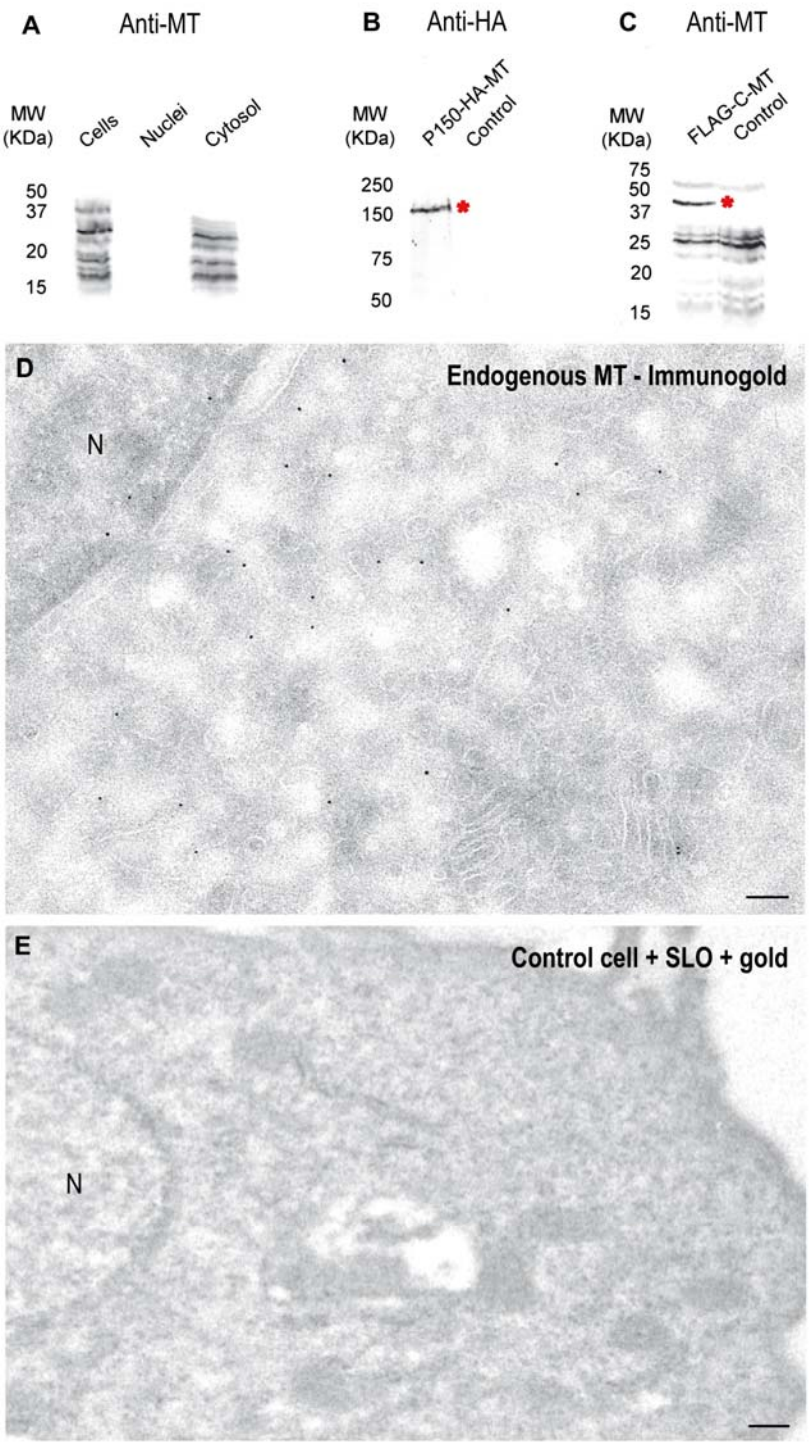

Figure S4 (related to Figure 2)

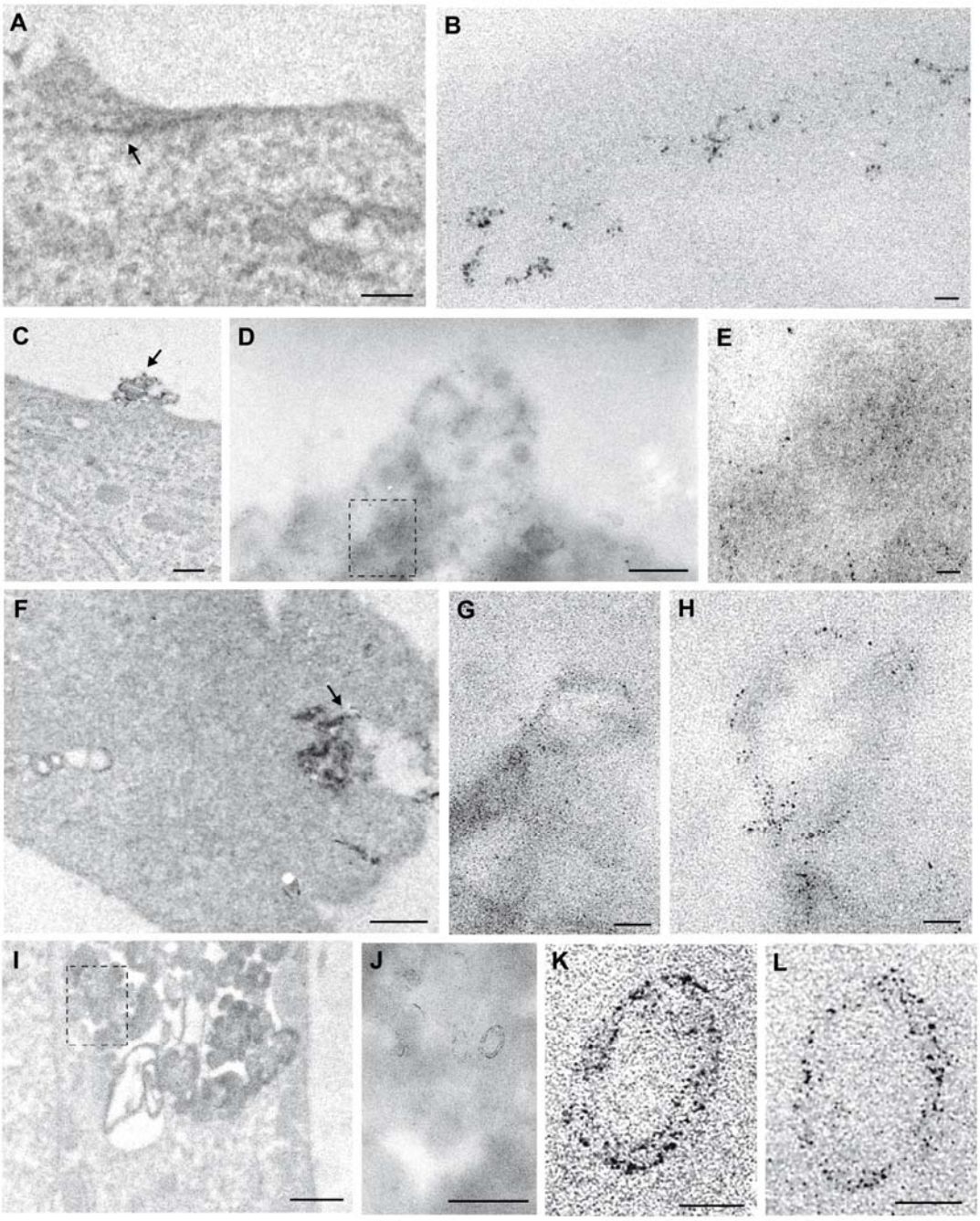

Figure S5 (related to Figures 2 and 4)

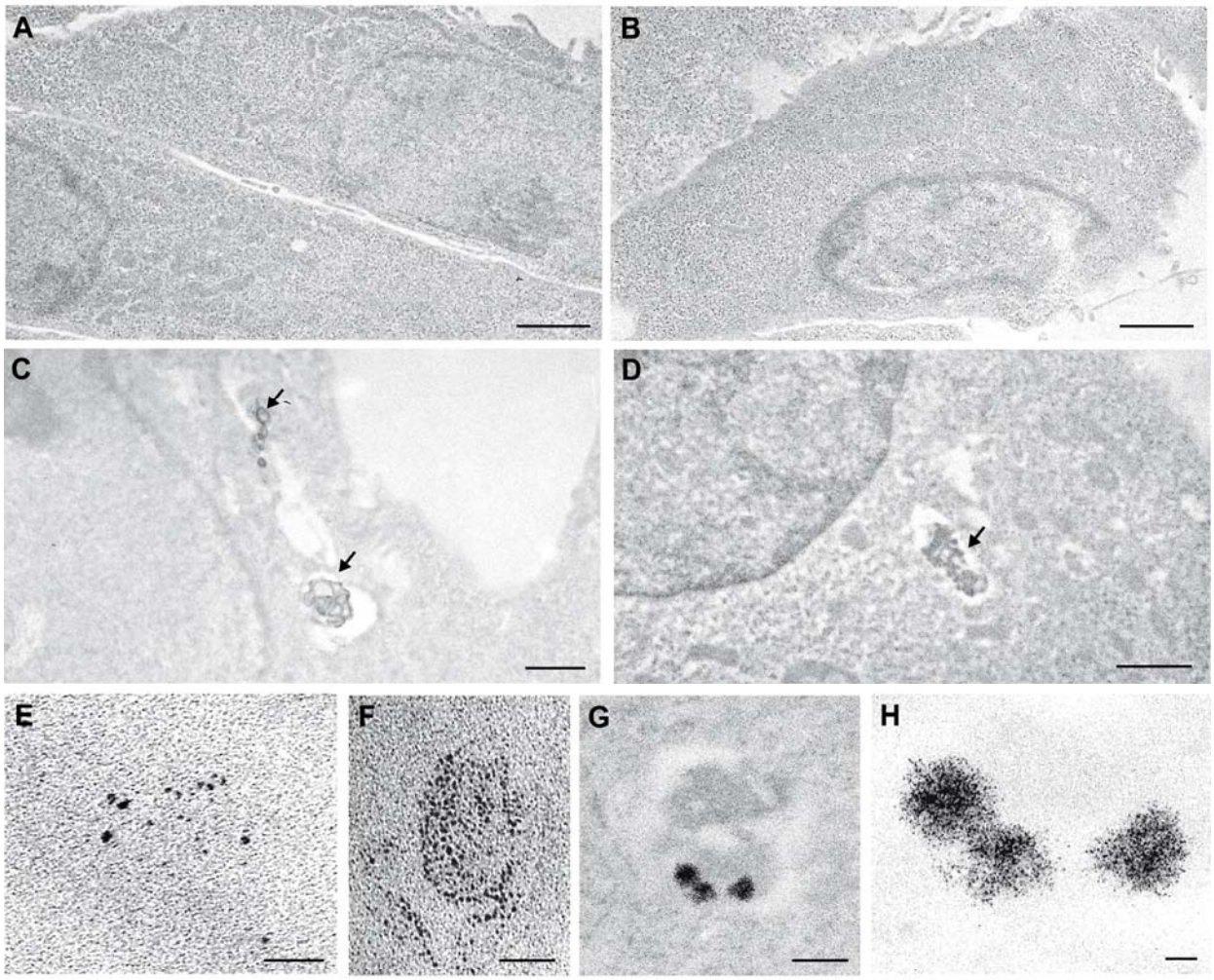

Figure S6 (related to Figure 4)

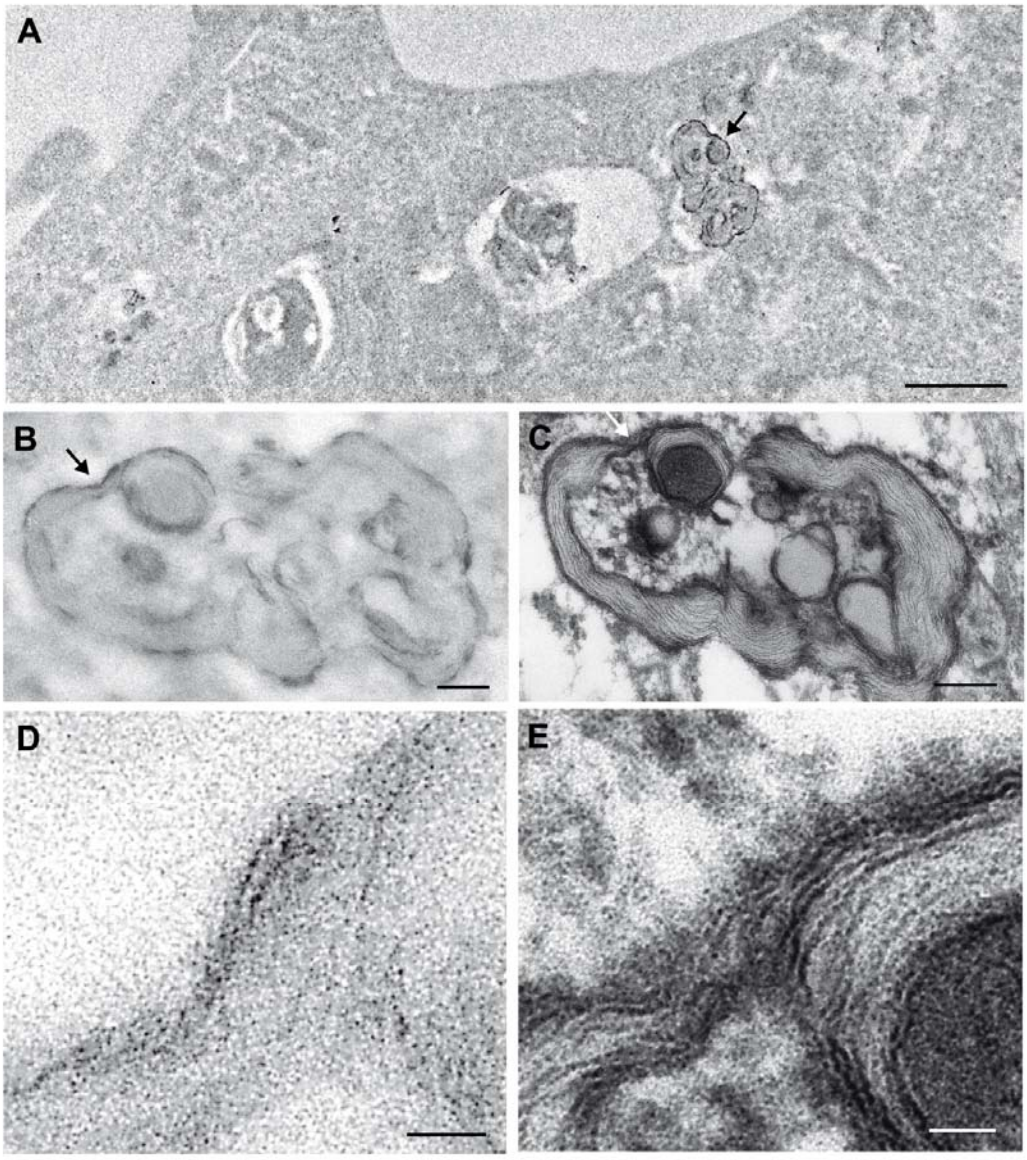

Supplemental figure Legends

Figure S1. Schematical organization of the RUBV genome, the plasmids and replicons used in this study (A) and confocal microscopy of transfected cells (B-E), related to Figures 1, 2, and 3. (A) Coding sequences are represented by open boxes and indicated by the name of the encoded nonstructural and structural RUBV proteins: P150, P90, C (capsid), envelope proteins E2 and E1. The various tags are represented by colored boxes: HA epitope (pink), MT (black), GFP (green), capsid sequences (grey). Picornavirus IRES elements to drive expression of neomycine resistance gene are indicated by blue asterisks. The coding sequence for the capsid protein tagged with the FLAG epitope and MT, expressed from pcDNA N961-MT is shown in red. (B) Fluorescence microscopy showing cytoplasmic filament arrays assembled by P150-GFP when expressed from plasmid in the absence of RUBV replicase protein P90. (C) Immunofluorescence detection of P150, co-expressed with replicase subunit P90 from replicon RUBrep-HA-MT/GFP. Green dots correspond to CPVs. (D) Immunofluorescence microscopy showing a dispersed cytoplasmic distribution of capsid expressed from pcDNA N961-MT plasmid and (E) recruitment of capsid to the CPVs in cells transfected with RUBrep-HA-MT/GFP replicon. Scale bars: 10 μm.

Figure S2. Biogenesis and ultrastructure of Rubella virus-induced organelles, related to Figures 2, 3, and 4. (A) A tentative schematic model based on previous observations (Fontana et al., 2007; Fontana et al., 2010; Spuul et al., 2010) and findings from the present study. Electron micrographs on the right show the ultrastructure of different virus-induced organelles described. (1) Replicase molecules accumulate in multillamellar convoluted structures associated to the plasma membrane (B) by an unknown mechanism. (2) These membranes are also seen inside vesicles close to the plasma membrane (C). (3) Perinuclear “early CPVs” with condensed membranes (D) and (E). (4) Late CPVs with recruited RER and characteristic vesicles, rigid membranes and dense domains (F) and (G). Scale bars: 0.5 μm.

Figure S3. Expression of endogenous MT, related to Figures 2 and 3. (A) Western blot analysis of whole cell extracts and nuclear and cytosolic fractions of BHK-21 cells using anti-MT antibodies. Multiple products corresponding to MT multimers are readily detected in whole cell extracts and cytosolic fractions, but are absent in the nuclear fractions. (B) Specific detection of replicase P150-HA-MT chimeric protein (asterisk) in cells, transfected with replicon RUBrep-HA-MT/GFP, by Western blot using anti-HA antibodies. No products were detected in untransfected control cells. (C) Western blot with anti-MT antibody showing expression of FLAG-MT-capsid (marked by an asterisk), and expression of endogenous MT in control and transfected cells (all other bands). (D) Endogenous MT in the cytosol of BHK-21 cells as detected by IEM performed on cryosections. Very few particles were seen in the nucleus (N). (E) Thin-section of a non-transfected cell, treated with SLO and AuCl, to serve as a negative control. No electron-dense clusters are detected. Scale bars: 100 nm for (D); 200 nm for (E).

Figure S4. Detection of MT-gold-P150 in plasma membrane and intracellular vacuoles, related to Figure 2. BHK-21 cells were transfected with the RUBrep-HA-MT/GFP replicon, treated with SLO and AuCl before fixing, and processing for thin sectioning. (A) Sections, including large planar areas of plasma membrane (arrow), contain randomly distributed groups of clusters as seen at higher magnification (B). Dense membranes protruding from the cell surface at low (C) and higher magnification (D) that contain numerous clusters, as seen in an enlargement of the area, marked with a dashed rectangle (E). (F), (G) and (H) Low, medium and high magnifications, respectively, of an intracellular vesicle near the plasma membrane. Enlargement in (H) shows groups of clusters inside the vesicle. (I) Dense vacuole containing groups of gold clusters with spherical-elliptical arrangements as seen at higher magnification in

(J) and (K). (L) Similar group of clusters from a different vacuole. Scale bars: 0.5 μm for (A), (C), (F) and (I); 25 nm for (B), (E), (H), (K) and (L); 200 nm for (D) and (J); 50 nm for (G).

Figure S5. Detection of MT-gold-tagged P150 in intact (non-SLO-permeabilized) cells treated with gold salts, related to Figures 2 and 4. TEM of ultra-thin sections of (A) mock-transfected BHK-21 cells, (B) mock-transfected cells, treated 30 min with 0.5 mM $AuCl_3$ and (C) and (D) cells, transfected with replicon RUBrep-HA-MT/GFP, and treated for 30 min with 0.5 mM $AuCl_3$. Note that the cell ultrastructure is not affected by the gold treatment and that electron-dense structures are seen in transfected cells exclusively (arrows in C and D). Here, gold nanoclusters concentrate in the plasma membrane (E), in vesicles close to the plasma membrane (F) and in perinuclear CPVs (G) as seen before in SLO-treated cells (compare to Figures 2 and S4). (H) Enlargement of (G) showing groups of clusters densely packed inside the CPV. Scale bars: 2 μm for (A) and (B); 1 μm for (C) and (D); 25 nm for (E), (F) and (H); 200 nm for (G).

Figure S6. Staining reveals fine details of organelles with MT-tagged proteins, related to Figure 4. BHK-21 cells, transfected with replicon RUBrep-HA-MT/GFP, were treated with $AuCl_3$ *in vivo* at 24 h post transfection. (A) Ultra-thin section of a cell, visualized by TEM without staining. Arrow indicates a vesicle with darker content, seen at higher magnification in (B). (C) Serial section of the same structure after uranyl acetate and lead citrate staining. (D) High magnification of the area, marked with a black arrow in (B), where gold nanoclusters can be distinguished. (E) High magnification of the area marked with a white arrow in (C), where staining reveals the multimembraneous nature of these structures. Scale bars: 1 μm for (A); 200 nm for (B) and (C); 25 nm for (D) and (E).

Supplementary Introduction

Immunogold labeling remains the main procedure for protein detection at the ultrastructural level, but antibodies are severely limited when high resolution and sensitivity are needed. The number of protein molecules detected by immunoelectron microscopy represents only a small fraction of the antigen in the cell. Post-embedding immunogold labeling is restricted to section surfaces, whereas pre-embedding procedures suffer from poor structural preservation, since cells must be permeabilized with detergents as to allow antibody access. Microinjection of antibodies was proposed as a potential solution, although limitations remain. Antibodies detect an unpredictable number of protein molecules within cells, depending on the accessibility of epitopes, which are often masked *in vivo* by interactions with other molecules. For these reasons, obtaining antibodies appropriate for immunoelectron microscopy has always been a difficult task. Moreover, the large size of the immune complexes inherently leads to poor resolution, as the distance between epitope and electron-dense marker is at least 15-20 nm, and new methods for efficient detection of macromolecules inside cells are urgently needed.